Photolithographic bio-patterning of magnetic sensors for biomolecular recognition

E. Albisetti[a,b], D. Petti[a,*], F. Damin[b], M. Cretich[b], A. Torti[a], M. Chiari[b], R. Bertacco[a]

[a] *L-NESS, Dipartimento di Fisica, Politecnico di Milano, Via Anzani 42, 22100 Como, Italy*
[b] *Istituto di Chimica del Riconoscimento Molecolare, CNR, Via Mario Bianco 9, 20131 Milan, Italy*

Received 13 December 2013
Received in revised form 5 March 2014
Accepted 17 April 2014
Available online 24 April 2014

1. Introduction

Since the first pioneering work by the Naval Research Laboratory group in 1998 [1], magnetoresistive biosensors based on the detection of biological entities labeled with magnetic beads have emerged as a promising new platform technology for biosensing. Giant magnetoresistance (GMR), tunneling magnetoresistance (TMR), anisotropic magnetoresistance (AMR) and Planar Hall Effect (PHE) sensors have been successfully applied to the detection of single magnetic particles [2–5] as well as to the focusing and detection of magnetic beads labeling target molecules in a biological sample [6]. In case of GMR devices, the detection of biomolecules with concentration down to the femtomolar [7] and zeptomolar [8] ranges has been achieved employing different techniques. The achievement of such extremely low limit of detection (LOD) essentially relies on two factors: (i) the optimization of the biochemistry connected to molecular recognition on the surface area, including the process of labeling with magnetic beads, and (ii) the optimization of the sensor sensitivity to magnetic beads.

The first issue deals with the implementation of a suitable biological assay for the target molecule (analyte) to be detected: sandwich immunoassay for proteins, direct single strand recognition for DNA or even competitive assays such as in the case of ELISA. More relevant for magnetoresistive biosensors is the detection scheme. In the so-called "post-hybridization method", initially used by the NRL group and adopted also in the present work, target biomolecules are labeled with biotin. First, molecular recognition between probes and targets takes place on the sensor surface, sometimes using a sandwich assay with the biotin attached to the second molecule sandwiching the analyte [9]. Then, magnetic beads coated with streptavidin are flushed over the sensors, allowing for a selective labeling of the sensor only where molecular recognition has taken place. In the magnetically assisted hybridization method, instead, target molecules are first labeled with beads which can then be used to magnetically concentrate the targets over the sensor area [10]. In this way lower LODs can in principle be achieved, thanks to pre-concentration, but the perturbation of the magnetic bead on the molecular recognition imposes the use of small nanoparticles. In this work, we will not deal with these biochemical aspects of the assays. Instead we will present an innovative method for patterning DNA probes only over the sensor area. This is related to the second fundamental issue for achieving a low LOD: the optimization of the sensor sensitivity to magnetic beads while keeping an almost linear response to their concentration.

In order to achieve such a high sensitivity, different aspects must be taken into account. First of all, the working point of the sensor must be carefully chosen in connection with the shape of the resistance vs. external field sensor transfer curve $R(H)$. The parameter

* Corresponding author. Tel.: +39 0313327308; fax: +39 0313327617.
E-mail address: daniela.petti@polimi.it (D. Petti).

to be maximized in case of lock-in detection and bead excitation by a small AC magnetic field does not coincide with the sensor sensitivity: $S_0 = (R\mu_0)^{-1}(dR/dH)$. The highest sensitivity to magnetic beads is indeed achieved by biasing the sensor in the region of its characteristics where the product between the DC bias field and the second derivative of $R(H)$ is maximum [11]. The second crucial aspect to be taken into account is the position and size of the biologically active area (i.e. the region where the biological probes are immobilized) with respect to the sensor. As it will be discussed in the following paragraphs, the average magnetic field generated by the beads over the sensor area strongly depends on their position, changing even its sign if generated by a particle inside or outside the sensor [12]. This raises issues in quantifying the immobilized beads upon biomolecular recognition, and thus in determining a straightforward relationship between the sensor signal and the analyte concentration. For this reason, controlling the beads distribution over the sensor, via selective patterning of probes, is critical for achieving a high and linear sensitivity to beads, which in turns ensures a low LOD.

Over the last decade, several methods for patterning biomolecules in micrometer size structures have been developed, such as micro contact printing [13], capillary force lithography [14], dip pen nanolithography [15] and nano-spotting [16]. A popular method for defining bio-active regions on magnetoresistive sensors is based on the selectiveness of thiol chemistry [7]. A gold layer is microfabricated and properly aligned over the sensor surface, and then selective gold functionalization is achieved thanks to spontaneous assembly of chemically reactive alkene thiols only on gold, thus leading to the formation of so called self-assembled monolayers (SAM) [17–19]. However, the formation of a well-assembled monolayer is not always straightforward, as it strongly depends on the purity of the alkanethiol being used. The presence of even low levels of contaminants can result in a disordered, non-ideal monolayer [20]. Furthermore, the additional step consisting in the microfabrication of a gold overlayer can be critical in terms of cost and compatibility with the sensor layout. In the great majority of cases, the gold layer constitutes an additional film above the insulating protecting layer which ensures biocompatibility and protects the sensor from the wet biological environment. This contributes to move the beads away from the active sensing layer, thus reducing the overall sensitivity.

Alternative strategies, not requiring the physical deposition and patterning of gold, consist in the use of photo-activated esters derived from N-hydroxysuccinimide (NHS) [21]. Patterning of aminohexyl modified DNA oligonucleotides is achieved through the selective photochemical reaction of a hydrogen-terminated silicon surface with alkenes functionalized with N-hydroxysuccinimide ester groups [22]. However, this technique is suitable only to silicon surfaces and the absence of a physical mask increases the risk of unspecific binding outside the patterned area.

In this paper, we present a novel approach to surface functionalization with micron or sub-micron resolution, which consists in the photolithographic patterning of a polymeric layer suitable for probe immobilization deposited by dip coating. The method presents relevant advantages with respect to state of the art techniques. Being optical lithography a widely accessible process, available in all microfabrication facilities, and providing sub-micron resolution, an easy scale up to mass production is possible. On the other hand, the use of a functional polymeric coatings compatible with many different substrates (e.g. SiO_2, Au, SiN, TiO_2, ...) [23] allows for a high flexibility and versatility, at variance with thiol-based chemistry which is strictly limited to gold. Finally, the use of an entirely wet process, including the polymer dip-coating and wet chemistry associated to photolithography, is fully compatible with low-cost massive production.

In our method a photoresist pattern acts as a mask for a peculiar self-adsorbent bioreactive polymer, which binds only to the areas of the chip surface not covered by the photoresist upon development in the organic solvent. In this way the subsequent DNA probe immobilization by spotting is effective only in the area coated by the polymer. The critical point of this approach is the need for organic solvents during the lithographic process which can denature probes immobilized on the polymeric coating. In case of DNA probes, however, their high stability even in organic solvents allows to easily overcome this issue. Being the polymer stable in acetone, its bioconjugation properties are not altered by the photoresist lift-off process which removes the photoresist while not affecting the DNA probe functionality for subsequent molecular recognition. In case labile probes are used, the spotting process can be performed after the lift-off procedure, so that any harsh chemical treatment on the probes is avoided. In principle this allows to extend this method to any kind of probe molecules.

The polymer used in this work is a reactive ter-copolymer obtained by radical polymerization of *N*,*N*-dimethylacrylamide (DMA), N-acryloyloxysuccinimide (NAS) and 3-(trimethoxysilyl) propyl methacrylate (MAPS), (DMA-MAPS-NAS).[24] This copolymer, introduced initially to immobilize oligonucleotides on the surface of microarray slides, suits the present application as (i) it forms a selective coating on the SiO_2 substrate by simple adsorption from an aqueous solution, not being affected by the photoresists proximity, (ii) it perfectly withstands lift-off in acetone.

The effectiveness of the proposed bio-patterning technique is demonstrated in DNA recognition experiments run in a microfluidic cell. The magnetic signal arising from molecular recognition events in bio-patterned sensors is found to be more than two times higher than in non-patterned sensors. This work demonstrates the huge potential of optolithographic bio-patterning for improving the quantification capability of magnetoresistive biosensors for molecular recognition. Besides, the very same technology for bio-patterning could be of high interest for many other biosensing approaches requiring on-chip probe immobilization over selected areas.

2. Materials and methods

2.1. Sensor and microfluidics

MTJ stacks with the structure (thicknesses in nm from now on) $Si/SiO_2(1000)/Ta(5)/Ru(18)/Ta(3)/Ir_{22}Mn_{78}(20)/Co_{60}Fe_{40}(2)/Ru(1.1)/Co_{40}Fe_{40}B_{20}(3)/MgO(2)/Co_{40}Fe_{40}B_{20}(1)/Ru(5)/Ta(5)$, were deposited by magnetron sputtering in an AJA Orion8 system with a base pressure of 2×10^{-9} Torr. CoFe and MgO layers were deposited in RF mode, while all the other layers were deposited in DC mode.

After the stack deposition, arrays of 8 MTJ sensors were fabricated using optical lithography and the same layout as in [11,25]. The junction areas were defined by ion milling in the shape of rectangles, with lateral dimensions of $2.5 \times 120\,\mu m^2$, where the shorter side is parallel to the magnetic easy axis of the pinned bottom reference layer, oriented along the *y*-axis in Fig. 1A. After e-beam evaporation of Cr(7)/Au(300) contacts, the samples were annealed at 330° C at a 10^{-6} Torr pressure for 1 h in a 400 mT magnetic field applied along the positive *y*-direction. Then, a $SiO_2(50)/Al_2O_3(80)/SiO_2(200)$ multilayer was deposited in RF mode from SiO_2 and Al_2O_3 targets to electrically insulate the sensor stack and protect it against fluids dispensed on the chip during the experiment. The $R(H)$ curve of a MTJ sensor is shown in Fig. 1B, for H applied parallel to the *y*-axis. The tunneling magnetoresistance is 50%, while the low-field sensitivity $S_0 = (R\mu_0)^{-1}(dR/dH)$ is 12%/mT in the linear region.

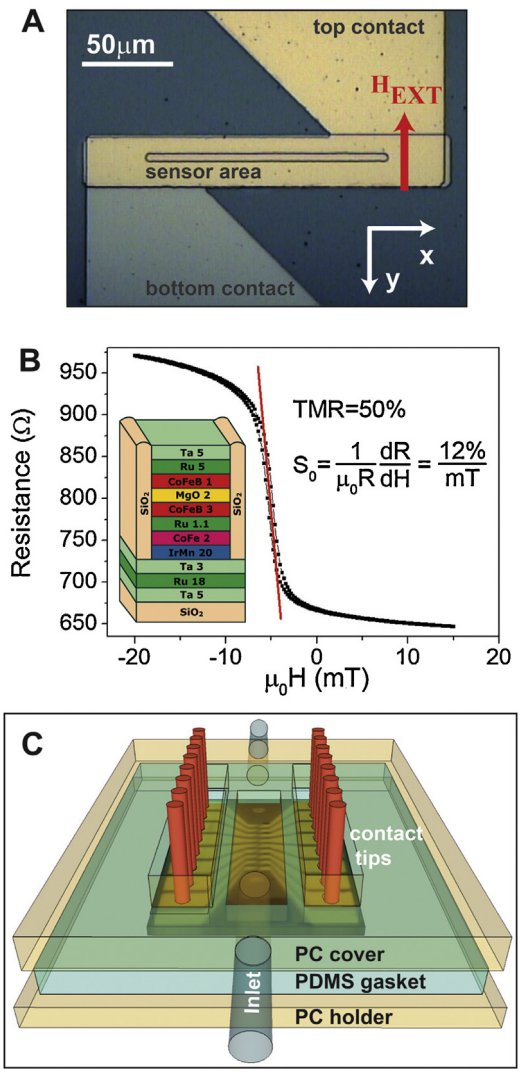

Fig. 1. (A) Optical image of a single sensor showing the geometry of the applied magnetic fields. (B) Sensor resistance $R(H)$ measured applying a 10 mV voltage across the junction. (C) Sketch of the microfluidic system providing also the electrical contact to the array of eight sensors.

The microfluidic apparatus (Fig. 1C) consists in a click-on cell comprising a Polycarbonate (PC) chip holder on top of which a 12 mm^3 microfluidic chamber is defined by a Polydimethylsiloxane (PDMS) gasket and a PC cover equipped with retractable tips for contacting the bottom and top electrodes of each sensor.

2.2. Biochemical reagents

Nanomag®-D, 250 nm diameter streptavidin coated magnetic beads, 75–80% (w/w) magnetite in a matrix of dextran (40 kD) were obtained from Micromod, Germany.

For the biotin–streptavidin binding and washing, phosphate buffer (PB) 0.1 M pH 7.4 with 0.02% of Tween20® was used.

TRIS, ethanolamine, SSC, ammonium sulfate, SDS, PBS, *N*,*N*-dimethylacrylamide (DMA) and [3-(methacryloyl-oxy)propyl] trimethoxysilane (MAPS) were purchased from Sigma (St. Louis, MO). *N*,-acryloyloxysuccinimide (NAS) was obtained from Polysciences (Warrington, PA). Oligonucleotides were synthesized by MWG-Biotech AG (Ebevsberg, Germany).

2.3. Probe immobilization, selective functionalization and oligonucleotides hybridization

In Fig. 2A the selective bio-functionalization process is sketched. $6 \times 120\,\mu m^2$ rectangles centered over the sensor areas were opened employing standard inverse optical lithography. After the spinning of a 1.4 μm thick layer of AZ 5214E photoresist (step 1), the sample underwent a soft baking at 110° C for 1′30″, followed by UV exposure (Hg I line (365 nm) of a mercury lamp) with a dose of 25.4 mJ/cm^2 through the photolithographic mask. Then, the sample underwent the reversal baking at 117 °C for 1′40″ and the flood UV exposure with a dose of 254 mJ/cm^2 (step 2). The sample was then developed for 20″ in AZ726MIF (step 3). The chip was then coated with a functional copolymer (step 4) made of dimethylacrylamide (DMA), *N*-acryloyloxysuccinimide (NAS) and 3-(trimethoxysilyl) propyl methacrylate (MAPS), copoly(DMA-MAPS-NAS). The copolymer synthesis procedure, first introduced by Pirri et al. [24], was recently revised by Sola et al. [26]. The coating provides active ester moieties suitable for immobilization of amino modified oligonucleotides and, at the same time, prevents non-specific adsorption of biological fluids components. The chip was immersed for 30 min in a 1% w/v solution of copoly(DMA-MAPS-NAS) in an aqueous solution of ammonium sulfate at 20% saturation then rinsed with water and dried under vacuum at 80 °C. The sensor areas were then entirely spotted (step 5) with a 23-mer synthetic oligonucleotide with the following sequence: 5′-GCCCACCTATAAGGTAAAAGTGA-3′, modified at the 5′ end with C_6 amino linker, giving rise to about 10^{12} binding sites per cm^2 on the chip surface [24]. The oligonucleotide was dissolved in 150 mM sodium phosphate buffer pH 8.5 at different final concentrations (ranging from 1 μM to 1 pM) and spotted using a non-contact microarray spotter SCENION sci-FLEXARRAYER S5 assembled with an 80 μm nozzle. Spot volume of each drop, temperature and humidity were 400 pL, 22 °C and 50% respectively. After overnight incubation in the humid chamber, allowing the oligonucleotide binding, the photoresist was stripped in acetone (step 6). Finally, the surface was blocked with a solution of bovine serum albumin (1% w/v) in phosphate saline buffer (PBS) for 1 h. This treatment prevents non-specific binding of biomolecules during the subsequent DNA hybridization phase.

In contrast, non-patterned sensors (i.e. the conventionally functionalized sensors) underwent only step 4 and 5 in Fig. 2A, followed by the final blocking step with BSA.

The sensor chip was then incubated with a complementary oligonucleotide target of sequence 5′-TCACTTTTACCTTATAGGTGGGC-3′, labeled with biotin at the 5′ end. The sensor surface was fully covered for 2 h with a 1 μM solution of the oligonucleotide target dissolved in the hybridization buffer (2× saline-sodium citrate (SSC), 0.1% w/v sodium dodecylsulphate (SDS) and 0.2 mg/ml of BSA). Finally, the chip was washed for 5 min with the washing solution (2× SSC, 0.1% w/v SDS), rinsed in 0.2× and 0.1× SSC buffer and dried under a nitrogen stream.

Reference sensors were spotted (in step 5) with an oligonucleotide having the same sequence of the target (5′-TCACTTTTACCTTATAGGTGGGC-3′) but modified at the 5′ end with a C_6 amino linker.

2.4. Magnetic labeling and detection

Magnetic nanoparticles dispersed in phosphate buffer (PB)-Tween solution (~10^8 particles/μl) and coated with streptavidin, were injected into the microfluidic cell at a flow rate of 50 μl/min. After filling the cell, the pump was switched off and we waited for 15 min to allow particle sedimentation, as well as selective immobilization over the sensor surface where the target molecules

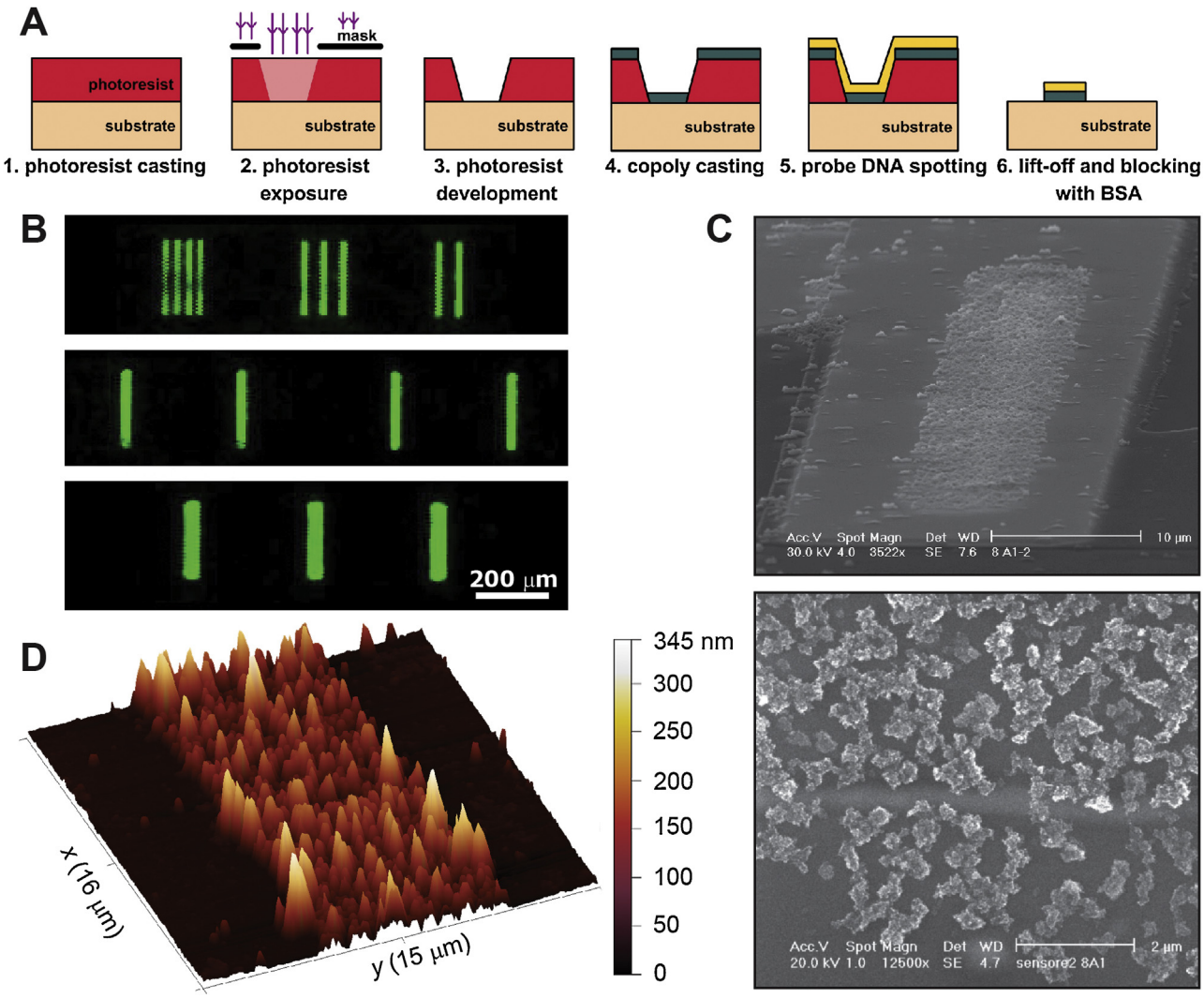

Fig. 2. (A) Sketch of the optolithographic process for the selective bio-functionalization. (B) Rectangular shapes on a Si/SiO_2 substrate, bio-patterned following the same procedure employed for the selective functionalization of the sensors. The fluorescence signal is given by a Cy3 dye labeling the complementary target DNA. (C) SEM images of the whole sensor area (top image) and zoomed view of the functionalized area (bottom) after the biomolecular recognition. In this case a 1 μM DNA target concentration was used. The selectively functionalized area is covered by the nanoparticles (250 nm Nanomag®-D) immobilized on the surface through the streptavidin biotin interaction. (D) AFM image of the sensor after biomolecular recognition and AFM profile: the peaks from 100 to 200 nm correspond to the nanoparticles that are fragmented after drying the chip.

exposed biotin. Finally, the sensor was washed several times with PB/Tween20 to remove unspecific, weakly bound magnetic nanoparticles. During all these operations the magnetoresistive response of the sensor was recorded. As it depends on the magnetic stray field from the beads, this allows monitoring the concentration of beads during the detection experiment and correlating it to the concentration of the target analyte.

The magnetoresistive signal was acquired through a double modulation technique in order to improve the sensor sensitivity and minimize the $1/f$ noise [27]. The current through the sensors was modulated at a frequency $f_1 = 1.101$ kHz by applying an AC voltage to the series of a load resistance (2 kΩ) and of the sensor connected to ground. The voltage drop across the sensor, proportional to the sensor resistance, was sent to the lock-in. An external magnetic field H_{ext} was applied parallel to the sensing axis, which corresponds to the y-direction in Fig. 1B. H_{ext} was the sum of two contributions: a DC field to bias the sensor in the optimum point of its characteristics [11] and a small oscillating field at $f_2 = 39$ Hz to excite the magnetic beads. Thanks to this double modulation, the sensor signal proportional to the concentration of beads above the sensor appears in the output voltage as a component at the frequency $(f_1 \pm f_2)$, which can be easily extracted via a lock-in amplifier.

A multiplexer was used to sequentially address the eight different sensors while current was permanently flowing through all the junctions, in order to ensure a good thermal stabilization.

3. Results and discussion

In order to assess the importance of the beads distribution on the sensor signal and identify the optimal area of the sensing surface, we simulated the magnetic field produced by beads at different positions over the sensor. Following previous works [12], we calculated the average magnetic field generated in correspondence of the sensor free layer by a single magnetic bead (MNP) magnetized along the y-direction, in suspension at a distance z above the chip surface. The last one is not flat, due to the presence of an additional SiO_2 layer (100 nm thick) outside the sensor area (3 μm wide), ensuring electrical insulation between the electrical contacts and the sensor plane. In the simulations this is taken into account considering two

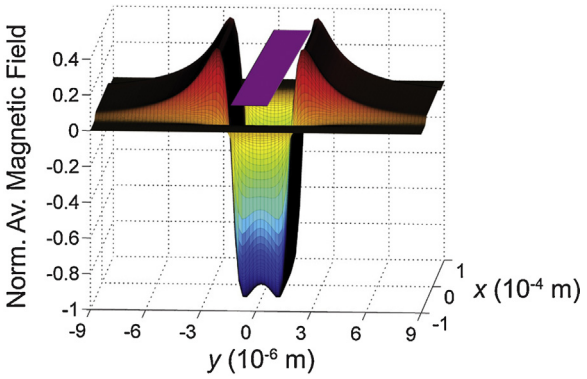

Fig. 3. Average magnetic field H_{DC} produced by a single bead on the sensor as a function of the bead position in the *xy* plane with respect to the $3 \times 120\ \mu m^2$ sensor area (in purple). For taking into account the actual geometry of the microfabricated sensor, we considered two different *z*-distances from the surface for beads outside ($z_o = 700$ nm) and upon the sensor area ($z_u = 600$ nm). (For interpretation of the references to color in this figure legend, the reader is referred to the web version of this article.)

different *z*-distances for beads outside ($z_o = 700$ nm) and upon the sensor area ($z_u = 600$ nm). In Fig. 3, the average magnetic field, normalized to the magnitude of the maximum average field H_{max}, is plotted as a function of the MNP position with respect to the center of the sensor. It is worth noting that the average field has the same sign as the external magnetizing field when the MNP is outside the sensor area and opposite sign when the MNP is above the sensor area. Therefore, considering a homogeneous distribution of beads (e.g. an infinite monolayer of MNP) at the same height *z* (constant) above the sensor, the positive and negative contributions perfectly compensate each other, thus giving rise to a not detectable signal. Furthermore, whereas the signal arising from the MNP above the sensor area is almost independent on the position, the contribution of MNPs outside the sensor area strongly depends on the MNP location, thus hindering a straightforward quantitative analysis. This calculation makes clear the importance of a micrometric precision on the spatial control over the beads distribution, both for maximizing the magnetic signal and for enabling accurate quantitative data analysis (check Ref. [28] for details about the calculations). From our calculations, the optimum width of the selectively functionalized area, centered on top of the sensor, should be about 3.7 μm. Indeed, in this condition, the beads within the functionalized area contribute to the total field with a signal of the same sign, thus maximizing their magnetic signal.

In order to experimentally validate these findings, DNA–DNA hybridization experiments were carried out using patterned magnetoresistive sensors coated and spotted according to the procedure described above. Before performing the magnetic detection experiments on selectively functionalized sensors, the effectiveness of the selective bio-patterning technique has been assessed on SiO_2/Si substrates and standard fluorescence experiments [29]. Rectangular-shaped areas with different dimensions were selectively functionalized with probe DNA and subsequently blocked with BSA as described in Section 2.3. The surfaces were then incubated with the complementary target DNA labeled with a Cy3 dye, following the same procedure employed for the sensors. Fig. 2B shows the fluorescence image of the patterns observed with a fluorescence scanner (ScanArray Lite, Perkin Elmer, MA, USA). The effectiveness of our technique in ensuring an extremely high contrast in the concentration of biomolecules inside and outside the patterns is confirmed by the absence of fluorescence outside the functionalized area in contrast with the strong signal inside the patterns. The ratio of the fluorescence intensity (proportional to the immobilized target DNA molecules) inside and outside the

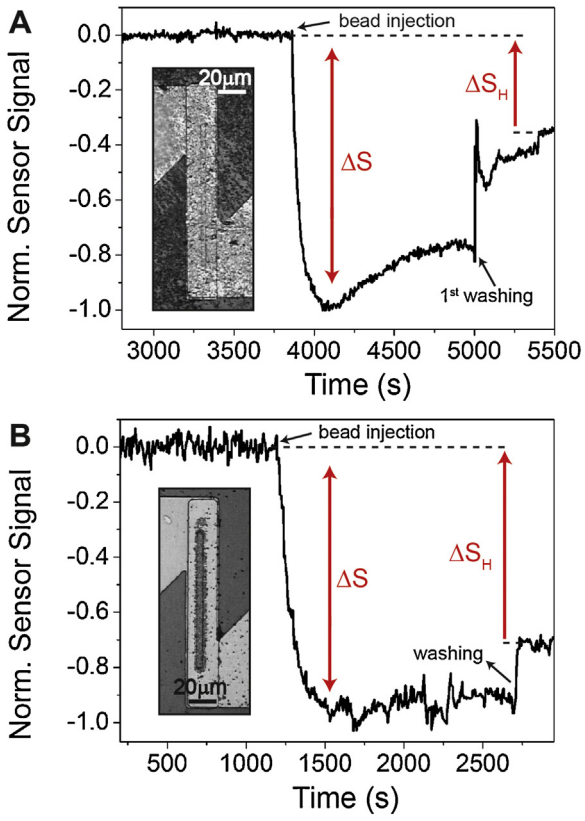

Fig. 4. Comparison between the normalized signal from the spotted (A) and selectively functionalized (B) sensors during a biomolecular recognition experiment. The binding signal is ΔS_H. In the inset: optical image of the sensor area after sedimentation.

bio-patterned areas is more than 320. In addition, the uniformity of the fluorescence signal within the single pattern and among different patterns indicates a good control and reproducibility of the process on a large scale.

Magnetic detection bioassays on both non-patterned and patterned magnetoresistive sensors have been performed, in order to compare their performances and correlate the results with the calculations.

The morphology of the bio-patterned sensor surfaces, after the molecular recognition assay, was evaluated by Scanning Electron Microscopy (SEM). Fig. 2C shows images taken at different magnification on the sensor area. In the top part, the whole bio-patterned region (which is located on top of the sensor area) is uniformly covered by the Nanomag®-D 250 nm diameter MNP used for labeling. It is worth noting the almost complete absence of MNP non-specifically bound to the surface outside the patterned area. In the bottom part, a zoom-view of the functionalized area shows the single MNPs and MNPs fragments bound to the surface. The MNP fragmentation occurs after the drying of the chip due to the fact that the MNPs are not stable in dry environment. An Atomic Force Microscopy (Fig. 2D) investigation shows peaks ranging from 50 nm up to 250 nm, thus confirming the uniform distribution of MNPs over the functionalized surface. The high specificity of the proposed method is confirmed by the low root mean square roughness (R_{RMS}) value of 4.26 nm calculated over a $5 \times 5\ \mu m^2$ non-functionalized area, which is comparable to the one measured on the bare sample, before the functionalization process (data not shown).

Typical signals from the magnetoresistive sensors during a DNA bioassay are shown in Fig. 4 and 5, normalized to the sedimentation signal ΔS. The baseline signal is initially acquired for 15–20 min and then streptavidin-coated beads are injected and let to settle

down. In our experimental configuration, the bead sedimentation leads to a decrease in the voltage signal as described in [11]. After saturation (i.e. full sedimentation), the beads are left to interact with the immobilized biotinylated target for 15 min. Finally, the chip is washed until the signal of the reference sensors in the array recovers its baseline and stays stable over time. The difference between the baseline and the final signal level in the other sensors is then proportional to the target concentration.

In Fig. 4 the detection of 1 μM of target concentration in case of conventional (panel A) and selective (panel B) functionalization is presented. In the insets, the optical images of the two sensors after performing the hybridization and washing steps are shown. The immobilized beads cover either the entire spotted area extending all around the sensor (Fig. 4A) or only a rectangle above the sensor active area in case of localized functionalization (Fig. 4B).

In both experiments A and B, the difference between the two baselines, before injecting the beads and after washing, gives the signal ΔS_H which is related to the concentration of target DNA immobilized on the sample surface. The absolute values of the signals, which are related to the same DNA target concentration, depend on the different sensor sensitivities arising from the intrinsic characteristic of each sensor. In order to allow a comparison, each ΔS_H signal is normalized to the bead sedimentation signal ΔS (see Fig. 4).

In case of conventional and selective functionalization, the $\Delta S_H/\Delta S$ ratios are 0.37 ± 0.01 for the non-patterned sensor and 0.75 ± 0.04 for the patterned one, indicating a twofold increase in the binding signal on the bio-patterned sensor. This is in nice agreement with our simulation of the sensor response shown in Fig. 3, which takes into account the actual sensor geometry. First we must consider that, due to some technical limitations, in these experiments the selectively functionalized area is about 6 μm wide. According to calculations presented in Fig. 3, we are thus exceeding the optimum width matching the flat negative part of the sensor response (3.7 μm for our sensor geometry, see above) and partially capturing the opposite signal coming from beads outside the active sensor area. Secondly, the bead distribution is not planar, because of the presence of an additional SiO_2 layer (100 nm thick) outside the sensor area (3 μm wide) (see above). This causes the beads immobilized over the sensor area to be closer to the sensor free layer and to generate a higher signal than those outside, placed 100 nm above. The different height of beads inside and outside explains why we can detect a non-negligible signal in case of non-patterned samples. Although a uniform, infinite, planar distribution of beads would give a zero net magnetic signal on the sensor area, the beads outside contribute here with a much lower signal than those upon the sensor area. From Fig. 3, the ratio between the signal from patterned and non-patterned sensors should be on the order of 3.6, which is in nice agreement with the experimental value of 2 if we consider that the bead distribution in both cases presents a sort of concentration on the sensor edges due to the stray field originating from the magnetic layers [11,28]. Apart from the sensitivity, it is worth noting another difference between the two signals. In case of non-patterned sensors (Fig. 4A), the positive sensor presents an increase of the signal after the initial sedimentation (around 4000 s), which is not a measurement artifact, since no thermal or electrical drift affect the baselines recorded before and after the experiment. Noteworthy, this signal rise is almost absent in the selectively functionalized sensors (Fig. 4B for 1 μM and Fig. 5A for 1 pM analyte concentration) as well as in the reference sensors (figure not shown). This suggests that the signal rise can be ascribed to the rearrangement of the beads upon the sensor area due to the chemical interaction with the functionalized surface. The initial pronounced signal decrease during sedimentation is due to the focusing action of the stray field of the sensors which attracts the beads mainly upon its area [11], giving rise to a negative

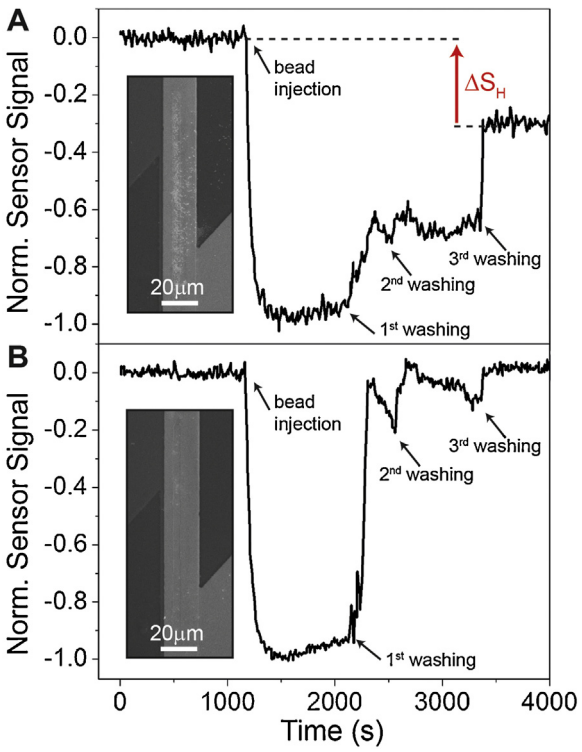

Fig. 5. Normalized signal from the positive (panel A) and reference (panel B) sensors. A 1 pM DNA target concentration was used. In the reference sensor, the baseline is recovered after the washing steps, while in the positive one the binding signal ΔS_H is highlighted. In the inset, SEM images of the two sensors after the experiment.

contribution to the total magnetic field sensed by the sensor (see Fig. 1B). Once the beads are in close proximity to the surface, a second mechanism takes place, i.e. the binding of the beads over the functionalized surface due to the streptavidin–biotin interaction. Due to chemically driven bead diffusion over the sensor chip, some of them move out of the sensor area and are immobilized there by chemical interaction. The signal rise after 4000 s, in Fig. 4A, can thus be ascribed to the immobilization of beads outside the sensor area, which partially cancels the negative signal coming from bead on top of the sensor. In the bio-patterned sensor this cancelation, and thus the rise in the signal, is absent because the bead immobilization takes place mainly upon the sensor area, where the beads contribute negatively to the sensor signal. The absence of this spurious signal evolution in patterned sensors is another advantage brought by selective bio-patterning.

The slight increase of the signal in the patterned reference sensor (lower panel in Fig. 5), which can be observed about 300 s after the signal drop due to the initial sedimentation, has a different origin. It is due to the sedimentation of beads outside the sensor area, which gives rise to a positive contribution to the sensor signal (see Fig. 3). The sedimentation outside the sensor area is slower than the sedimentation upon the sensor area, because of the absence of the focusing effect of the sensor stray field. Therefore, bead sedimentation outside the sensor (and thus the slow increase in the positive contribution to the signal) keeps going also after the sedimentation on top of the sensor reached saturation.

The good yield of the selective functionalization process and the reproducibility of the experiment have been confirmed by performing biomolecular recognition experiments on other selectively bio-functionalized sensor chips, acquiring the signal coming from three different sensors sequentially. Also, the characteristic curve of the $\Delta S_H/\Delta S$ signal for different target DNA concentrations is provided (see Supplementary material). Fig. 5 shows the results

obtained on a chip employing the same selective functionalization protocol described above, for 1 pM concentration of the target DNA used in the bioassay. The sensor and reference signals during the experiment are respectively reported in panels A and B of Fig. 5. In the insets, the SEM images of the sensor surface after the bioassay are reported. In this case the binding signal $\Delta S_H/\Delta S$ is 0.31 ± 0.02 and is obtained after several washing steps, allowing a full recovery of the baseline signal in the reference sensor. The absence of beads in panel B of Fig. 5 confirms that multiple washes are effective in removing the non-specifically bound beads. By comparing the ΔS_H signals from the positive and reference sensors, after normalization to the sedimentation signal ΔS, it is possible to calculate the bioassay signal to background ratio for a pM concentration of the analyte: $S/N_b = 23$. This clearly indicates that selective bio-patterning coupled to our MTJ based magnetoresistive sensors allows to achieve a limit of detection largely below 1 pM, i.e. in the fM range, without pre-concentration of the target. To our knowledge, while with magnetoresistive sensors and assisted hybridization a limit of detection of 1 fM has been reached [7], without target focusing detection of DNA concentrations only in the pM range [7,30] or higher [31] has been demonstrated so far. In this context, our results indicate that coupling selective functionalization with MTJ based magnetic sensors provides a suitable biosensing platform for highly sensitive, quantitative DNA recognition.

4. Conclusions

In this paper we reported on a straightforward photolithographic technique which allows the realization of micron-sized bio-patterned areas exploiting a lift-off resistant bio-reactive polymer. Such technique was employed to selectively functionalize arrays of MTJ-based magnetoresistive biosensors. DNA detection bioassays were run in a controlled microfluidic environment, both with patterned and non-patterned sensors.

A sizable enhancement of the magnetic biosensing platform performances, in terms of sensitivity and signal stability, can be achieved through the proper selection of the functionalized area. In particular we observed a twofold increase of the binding signal from selectively functionalized sensors with respect to the conventionally functionalized ones. Exploiting selective bio-patterning a LOD below 1 pM has been found in case of DNA detection without target pre-concentration. This remarkable result indicates the relevance of our selective bio-patterning method for improving the quantification capabilities and LOD of magnetoresistive biosensing platforms. In addition, more generally, our approach provides an easy and effective solution to the present technological need of highly controlled immobilization of biomolecules in micron-sized areas of biochips, biosensors and LOC devices.

Acknowledgments

This work was funded by Fondazione Cariplo via the project SpinBioMed (Project No. 2008.2330). E.A., D.P. and R.B. acknowledge Elisa Sogne for the improvement of the lithographic processes and Massimiliano Bianchi and Monica Bollani for the SEM images.

Appendix A. Supplementary data

Supplementary data associated with this article can be found, in the online version.

References

[1] D.R. Baselt, G.U. Lee, M. Natesan, S.W. Metzger, P.E. Sheehan, R.J. Colton, A biosensor based on magnetoresistance technology, Biosens. Bioelectron. 13 (1998) 731–739.
[2] W. Shen, X. Liu, D. Mazumdar, G. Xiao, In situ detection of single micron-sized magnetic beads using magnetic tunnel junction sensors, Appl. Phys. Lett. 1 (2005) 5–17.
[3] R.C. Chaves, D. Bensimon, P.P. Freitas, Single molecule actuation and detection on a lab-on-a-chip magnetoresistive platform, J. Appl. Phys. 109 (2011) 064702.
[4] P.P. Freitas, R. Ferreira, S. Cardoso, F. Cardoso, Magnetoresistive sensors, J. Phys. Condens. Matter. 19 (2007) 165221–165242.
[5] L. Ejsing, M.F. Hansen, A.K. Menon, H.A. Ferreira, D.L. Graham, P.P. Freitas, Planar Hall effect sensor for magnetic micro- and nanobead detection, Appl. Phys. Lett. 84 (2004) 4729.
[6] M. Donolato, M. Gobbi, P. Vavassori, M. Leone, M. Cantoni, V. Metlushko, et al., Nanosized corners for trapping and detecting magnetic nanoparticles, Nanotechnology 20 (2009) 385501.
[7] V.C. Martins, F.A. Cardoso, J. Germano, S. Cardoso, L. Sousa, M. Piedade, et al., Femtomolar limit of detection with a magnetoresistive biochip, Biosens. Bioelectron. 24 (2009) 2690–2695.
[8] R.S. Gaster, L. Xu, S.-J. Han, R.J. Wilson, D.A. Hall, S.J. Osterfeld, et al., Quantification of protein interactions and solution transport using high-density GMR sensor arrays, Nat. Nanotechnol. (2011) 4–10.
[9] S.J. Osterfeld, H. Yu, R.S. Gaster, S. Caramuta, L. Xu, S.-J. Han, et al., Multiplex protein assays based on real-time magnetic nanotag sensing, Proc. Natl. Acad. Sci. USA 105 (2008) 20637–20640.
[10] H.A. Ferreira, D.L. Graham, N. Feliciano, L.A. Clarke, M.D. Amaral, P.P. Freitas, Detection of cystic fibrosis related DNA targets using AC field focusing of magnetic labels and spin-valve sensors, IEEE Trans. Magn. 41 (2005) 4140–4142.
[11] E. Albisetti, D. Petti, M. Cantoni, F. Damin, A. Torti, M. Chiari, et al., Conditions for efficient on-chip magnetic bead detection via magnetoresistive sensors, Biosens. Bioelectron. 47 (2013) 213–217.
[12] G. Li, S. Sun, S.X. Wang, Spin valve biosensors: signal dependence on nanoparticle position, J. Appl. Phys. 99 (2006) 08P107.
[13] S. Alom Ruiz, C.S. Chen, Microcontact printing: a tool to pattern, Soft Matter. 3 (2007) 168.
[14] K.Y. Suh, H.H. Lee, Capillary force lithography: large-area patterning, self-organization, and anisotropic dewetting, Adv. Funct. Mater. 12 (2002) 405–413.
[15] K. Mitsakakis, S. Sekula-Neuner, S. Lenhert, H. Fuchs, E. Gizeli, Convergence of dip-pen nanolithography and acoustic biosensors towards a rapid-analysis multi-sample microsystem, Analyst 137 (2012) 3076–3082.
[16] M. Breitenstein, P.E. Nielsen, R. Hölzel, F.F. Bier, DNA-nanostructure-assembly by sequential spotting, J. Nanobiotechnol. 9 (2011) 54.
[17] A. Ulman, Formation and structure of self-assembled monolayers, Chem. Rev. 96 (1996) 1533–1554.
[18] J.C. Love, L.A. Estroff, J.K. Kriebel, R.G. Nuzzo, G.M. Whitesides, Self-assembled monolayers of thiolates on metals as a form of nanotechnology, Chem. Rev. 105 (2005) 1103–1169.
[19] A.B. Steel, T.M. Herne, M.J. Tarlov, Electrochemical quantitation of DNA immobilized on gold, Anal. Chem. 70 (1998) 4670–4677.
[20] C.-Y. Lee, H.E. Canavan, L.J. Gamble, D.G. Castner, Evidence of impurities in thiolated single-stranded DNA oligomers and their effect on DNA self-assembly on gold, Langmuir 21 (2005) 5134–5141.
[21] M. Yang, R.L.M. Teeuwen, M. Giesbers, J. Baggerman, A. Arafat, F.A. de Wolf, et al., One-step photochemical attachment of NHS-terminated monolayers onto silicon surfaces and subsequent functionalization, Langmuir 24 (2008) 7931–7938.
[22] H.B. Yin, T. Brown, J.S. Wilkinson, R.W. Eason, T. Melvin, Submicron patterning of DNA oligonucleotides on silicon, Nucleic Acids Res. 32 (2004) e118.
[23] D. Petti, A. Torti, F. Damin, L. Sola, M. Rusnati, E. Albisetti, et al., Functionalization of gold surfaces with copoly(DMA-NAS-MAPS) by dip coating: surface characterization and hybridization tests, Sens. Actuators B: Chem. 190 (2014) 234–242.
[24] G. Pirri, F. Damin, M. Chiari, E. Bontempi, L.E. Depero, Characterization of a polymeric adsorbed coating for DNA microarray glass slides, Anal. Chem. 76 (2004) 1352–1358.
[25] M. Donolato, E. Sogne, B.T. Dalslet, M. Cantoni, D. Petti, J. Cao, et al., On-chip measurement of the Brownian relaxation frequency of magnetic beads using magnetic tunneling junctions, Appl. Phys. Lett. 98 (2011) 073702.
[26] L. Sola, M. Chiari, Modulation of electroosmotic flow in capillary electrophoresis using functional polymer coatings, J. Chromatogr. A 1270 (2012) 324–329.
[27] S.-J. Han, L. Xu, R.J. Wilson, S.X. Wang, A novel zero-drift detection method for highly sensitive GMR biochips, IEEE Trans. Magn. 42 (2006) 3560–3562.
[28] E. Albisetti, D. Petti, F. Damin, M. Cretich, M. Bagnati, L. Sola, et al., Optimization of the bio-functionalized area of magnetic biosensors, Eur. Phys. J. B. 86 (2013) 261.
[29] G. Oliviero, P. Bergese, G. Canavese, M. Chiari, P. Colombi, M. Cretich, et al., A biofunctional polymeric coating for microcantilever molecular recognition, Anal. Chim. Acta 630 (2008) 161–167.
[30] L. Xu, H. Yu, S.-J. Han, S. Osterfeld, R.L. White, N. Pourmand, et al., Giant magnetoresistive sensors for DNA microarray, IEEE Trans. Magn. 44 (2008) 3989–3991.
[31] J. Schotter, P. Kamp, A. Becker, A. Pühler, G. Reiss, H. Brückl, Comparison of a prototype magnetoresistive biosensor to standard fluorescent DNA detection, Biosens. Bioelectron. 19 (2004) 1149–1156.